Device-Independent Representation of Photometric Properties of a Camera

Anonymous CVPR submission

Paper ID ****

Abstract

In this paper we propose a compact device-independent representation of the photometric properties of a camera, especially the vignetting effect. This representation can be computed by recovering the photometric parameters at sparsely sampled device configurations(defined by aperture, focal length and so on). More importantly, this can then be used for accurate prediction of the photometric parameters at other new device configurations where they have not been measured.

1. Introduction

In this paper we present a device independent representation of the photometric properties of a camera, in particular the vignetting effect. The photometric properties of a camera consist of the intensity transfer function, commonly called the *response curve*, and the spatial intensity variation, marked by a characteristic intensity fall-off from the center to fringe, commonly called the *vignetting effect*.

Cameras are common today in many applications including scene reconstruction, surveillance, object recognition and target detection. They are also used extensively in many projector camera applications like scene capture, 3D reconstruction, virtual reality, tiled displays, and so on. In a research and development environment the same camera may be used for several different applications and different settings. But for each particular scenario, we need to calibrate this camera anew when properties like vignetting effect or response curve depend only on device parameters and change very slowly, if at all, with time. Photometric calibrations are often time consuming and may need specific patterns and conditions which are hard to generate (e.g. diffused object illuminated in a diffused manner).

We design a compact device-independent representation of the non-parametric photometric parameters in a space spanned by the device settings like aperture and focal lengths. We propose a higher-dimensional Bezier patch for our device-independent representation based on the critical observation that the photometric parameters of a camera change smoothly across different device configurations. The primary advantages of this representation are the following: (a) generation of an *accurate representation* using the measured photometric properties at a few device configurations obtained by *sparsely sampling* the device settings space; (b) *accurate prediction* of the photometric parameters from this representation at unsampled device configurations. To the best of our knowledge, we present the first device independent representation of photometric properties of cameras which has the capability of predicting device parameters at configurations where it was not measured.

Our device independent representation opens up the opportunity of factory calibration of the camera and the data then being stored in the camera itself. Our compact representation requires very small storage. Further, the predictive nature of our model assures that properties at many different settings can be accurately generated from this representation. Finally, our Bezier based representation can be easily computed using a inexpensive embedded hardware allowing on-the-fly generation of the photometric properties at different device settings which can then be used to correct the imagery in real-time.

2. Related Work

There are many methods that use a parametric model to represent and estimate the camera response curve [16, 18, 7, 25, 20, 10, 11, 6]. [4, 15] use a non-parametric model for estimating the response curve. Other methods estimate the vignetting effect of a camera when the response curve is known using a parametric model [1, 29, 28, 26, 2, 23, 3, 5, 30]. The problem of estimating an unknown response curve and the vignetting effect of the camera is an underconstrained one. [12, 13, 9] estimate both the response curve and the vignetting effect simultaneously using parametric models, and can recover the vignetting effect only up to an exponential ambiguity.

The changes in the photometric properties of a camera depend on a large number of unforseen physical parameters, especially in today's inexpensive highly miniaturized devices which often undergo adverse optical aberrations due to low quality material properties. Hence, almost all of the

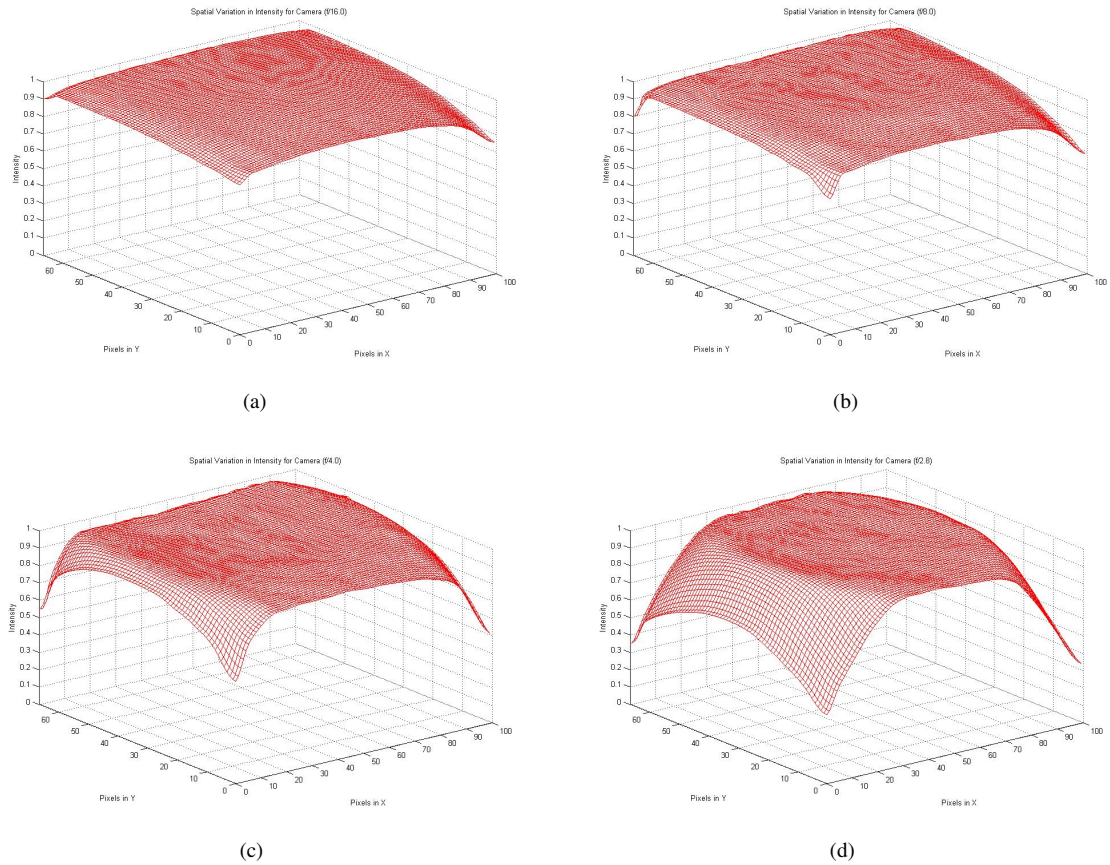

(a) (b)

(c) (d)

Figure 1. The camera vignetting effect estimated at (a) f/16, (b) f/8, (c) f/4 and (d) f/2.8. Note that the vignetting effect gets more pronounced as the aperture size increases from (b) to (d).

models for the photometric properties mentioned above are *device-dependent* physically-based model of the response curve and the vignetting effect. Accounting for all these physical influences accurately is very difficult in a device-dependent model. Hence, many simplifying assumptions are made (like principal center coincides with the image center, the vignetting is a polynomial function of the radius and so on), which are often not true physically.

Contrary to these models, we seek a *device-independent* representation defined in a multi-dimensional space spanned by the several controllable device settings like aperture and focal length. Hence, our model precludes any such assumptions common in device dependent models. Since it depends only on the device settings, it is easily scalable to large number of device settings. Our method can easily be applied when the estimated parameters are in non-parametric form as in [4, 15]. More recently, there have been works which constrain the under-constrained problem of finding response curve and vignetting effect of a camera by introducing a projector in a closed feedback loop where the projected input images seen by the camera are known [8, 24]. These can thus estimate the response curves and vignetting effects of both the camera and the projector simultaneously. These methods use non-parametric representations of the photometric properties particularly suited for our representation. For methods that use parametric representation, a intermediate non-parametric representation can be easily generated to make it conducive to our device independent representation.

3. Device-Independent Representation

In this section we present a new and efficient device independent representation of the photometric properties of a camera.

We seek a *device-independent* representation with the following goals. First, the representation should be defined in a multi-dimensional space spanned by the controllable device settings like aperture and focal length. We call this space as the *device settings space*. Second, the representation should be *compact*. Third, it should be easy to compute the parameters of the representation by estimating the photometric properties (response curve and vignetting effect) at *sparsely sampled* points in the device settings space. Fi-

nally, the photometric parameters at new points on the device settings space (where it was not measured) should be *predicted* easily and accurately from this compact representation.

Our representation of photometric camera properties and its efficient one-time evaluation can have a significant impact in the performance of projector-camera or capture systems. Currently, the camera used in such systems are not corrected for their vignetting effect due to difficult calibration processes. So, usually only a small central part of the image is considered to avoid whatever vignetting effect is present. To avoid this inefficiency in making use of the whole resolution of the camera, more often the camera is set to low aperture (f/16 or lower) [4] where the vignetting is considered insignificant. But this results in noisy images due to low light. Allowing more light without changing the aperture setting is only possible via a higher shutter speed. But, in this case, the camera cannot tolerate movements leading to motion-blurred images. Our method can now enable using factory-calibrated cameras in any setting appropriate for the demands made by the application.

Of the photometric properties, the response curve is spatially invariant and the vignetting effect is input invariant. Usually vignetting shows changes from one device setting to another, while the response curve remains the same [4, 14]. So, in our discussion, we only consider the vignetting effect assuming a compact polynomial representation for the 1D response curve. First, we describe our method for two controllable device settings in our cameras, focal length and aperture. This will be followed by a generalization of the scheme to allow more device settings. Figure 1 provides an example of the input to our method – the vignetting effect of the camera at different aperture settings.

We desire to represent the vignetting effect of the camera as a function $C(u, v, f', a')$ that returns the vignetting effect at spatial coordinate (u, v) for device settings parameters of focal length, f, and aperture, a. We call the 2D space spanned by f and a as the device settings space. f' and a' are functions of f and a and provide a parametrization of the device settings space most suited for finding C. This will be explained in details in Section 3.1.

Our representation for the vignetting effect C is based on the critical observation that it changes smoothly and coherently with change in device settings and with spatial coordinates. Hence, we choose a 4 dimensional Bézier surface to represent this compactly. We define the Bézier surface $C(u, v, p_f, p_a)$ as

$$\sum_{i=0}^{N_u}\sum_{j=0}^{N_u}\sum_{k=0}^{N_f}\sum_{l=0}^{N_a} B_i(u)B_j(v)B_k(f')B_l(a')P_{i,j,k,l}$$

$$= \sum_{i=0}^{N_u}\sum_{j=0}^{N_v}\sum_{k=0}^{N_f}\sum_{l=0}^{N_a} B_{i,j,k,l}(u, v, f', a')P_{i,j,k,l}$$

where u,v,f' and a' are normalized in $[0, 1]$, $P_{i,j,k,l}$ are the control points of the Bézier. B_i's are the Bernstein polynomials described by:

$$B_i(u) = \binom{N_u}{i} u^i(1-u)^{N_u-i} \quad (1)$$

Note that in the above equations, N_u, N_v and N_a and N_f can be different. This assures that the smoothness of the Bézier can be different in the domains of u, v, f' and a'. For example, in a very high-end camera, if the vignetting is very limited, it may suffice to have $N_u = N_v = 3$, but it may change over the aperture setting to result in $N_a = 4$.

Our method involves three steps: (a) First, the device settings space spanned by f and a is *sparsely sampled*. The self calibration method mentioned in the previous section is used to estimate the vignetting effect at these sparsely sampled device settings. (b) Second, the device parameters f and a are *parameterized* between $[0, 1]$ to yield the parameters f' and a' respectively that will be used to parameterize the fitting of the Bézier. (c) Third, a four dimensional Bézier surface $C(u, v, f', a')$ is *fitted* to this data and the control points, $P_{i,j,k,l}$ are estimated from the fitted function. (c) Finally, the vignetting effect at an unknown device configuration is *predicted* by evaluating the fitted $C(u, v, f', a')$ at the new device settings.

3.1. Parametrization

The parametrization of *device settings parameters* f and a to the *normalized parameters* p_f and p_a that range between 0 and 1 is critical to achieve a good fit for C and is described in details in this section.

Let us assume that the device settings parameter f and a are sampled at F and A values respectively. These are $f_1, f_2, \ldots, f_F$ and $a_1, a_2, \ldots, a_A$ respectively. Thus, the total number of sampled device configurations in the device settings space is given by $F \times A$. We estimate the vignetting effect using the self-calibration technique at each of the $F \times A$ device configurations.

We first consider iso-parametric curves for f i.e. a curve where a is constant. Note that there will be A such iso-parametric curves. Let us consider one such iso-parametric curve where $a = a_1$. The distance between adjacent normalized parametric values at (f_i, a_1) and (f_{i+1}, a_1) on this curve is assigned in such a way that they are proportional to the distance between the two dimensional surfaces representing the vignetting effect at these two device settings of (f_i, a_1) and (f_{i+1}, a_1), estimated using the self calibration technique. For measuring the distance between two surfaces we used the L_∞ distance (maximum distance) between them. Note that this parametrization is a *non-linear* monotonically increasing function of both f and a. We denote this by $f' = p_f(f, a)$ and $a' = p_a(f, a)$. Further, a uniform sampling of the device settings space spanned by f

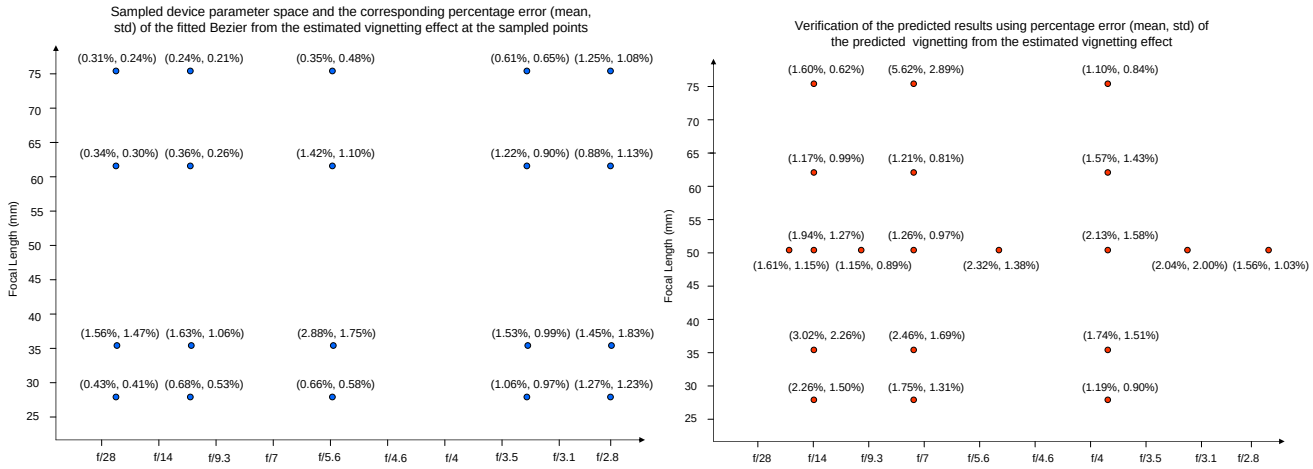

(a) (b)

Figure 2. (a) This plot shows the sampling of the devices parameter space using for recovering the Bezier function and the corresponding mean and std error of the fitted vignetting from the estimated vignetting at the sampled settings. (b) This plot shows the device parameters where we verified our prediction method and the corresponding mean and std errors of the predicted vignetting from the estimated vignetting at these settings.

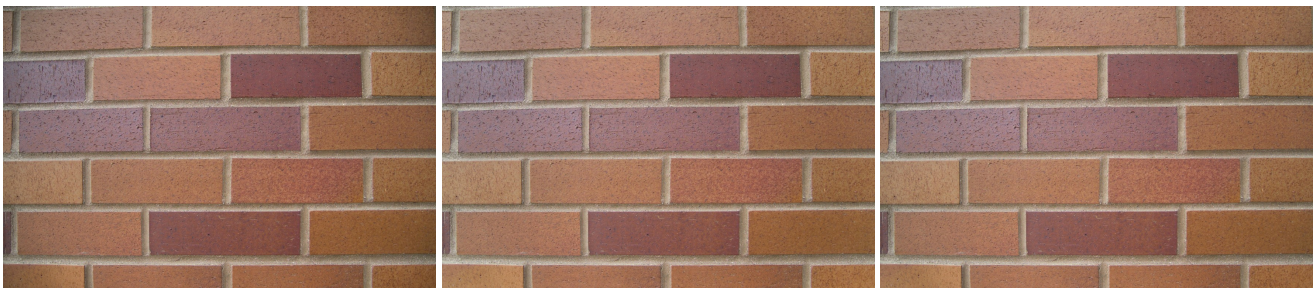

(a) (b) (c)

Figure 3. Comparison of vignetting correction: (a) uncorrected image captured at f/3.3 (b) corrected image using actual vignetting effect from calibration (c) corrected image using predicted vignetting effect.

and a does not assure an uniform sampling of the normalized parameter space spanned by f' and a'.

After f and a are parameterized to f' and a' as above, we fit a four dimensional Bézier using linear least squares to estimate $C(u, v, f', a')$ and the control points $P_{i,j,k,l}$ thereof.

3.2. Prediction

Once the function $C(u, v, f', a')$ is estimated, we use it to predict the vignetting at a new device configuration (f_{new}, a_{new}). The most critical aspect of this prediction is the parametrization of these new device settings (f_{new}, a_{new}) to (f'_{new}, a'_{new}) that will yield accurate prediction from the fitted $C(u, v, f', a')$. This in turn depends on how the functions p_f and p_a are approximated. We tried both global and local approximation techniques with similar results. These are summarized in the next section.

3.3. Experiments

We have experimented our representation on two cameras: a high-resolution (3.4-13.5 Megapixels) expensive camera like the Kodak DCS and an low-resolution (VGA) Point Grey camera with similar results. We found that a surface of at least degree 4 is needed in both cases. Hence, $N_u = N_v = N_1 = N_2 = 4$.

To reconstruct the Bézier function $C(u, v, f', a')$, we used 5 samples of the aperture settings at f/22, f/11, f/5.6, f/3.3 and f/2.8 ($A = 5$) and four samples of focal length at 28mm, 35mm, 62mm and 75mm ($F = 4$). Thus, we estimate the vignetting effect using our self-calibration procedure at $F \times A = 20$ device configurations. This sampled device settings are illustrated in Figure 2(a) demonstrating that estimation of the vignetting effect is required only at a few sparse samples in the device settings space. We assume the vignetting effect at a smaller aperture, say f/32.0, is negligible and include a flat surface at this aperture for our data

Table 1. Percentage error of the fitted four dimensional Bézier function of degree 4 from the vignetting effect estimated using the self-calibration method.

focal length	f/Stop	Mean	STD
28mm	f/2.8	1.27%	1.23%
28mm	f/3.3	1.06%	0.97%
28mm	f/5.6	0.66%	0.58%
28mm	f/11.0	0.68%	0.53%
28mm	f/22.0	0.43%	0.41%
35mm	f/2.8	1.45%	1.83%
35mm	f/3.3	1.53%	0.99%
35mm	f/5.6	2.88%	1.75%
35mm	f/11.0	1.63%	1.06%
35mm	f/22.0	0.56%	0.47%
62mm	f/2.8	0.88%	1.13%
62mm	f/3.3	1.22%	0.90%
62mm	f/5.6	1.42%	1.10%
62mm	f/11.0	0.36%	0.26%
62mm	f/22.0	0.34%	0.30%
75mm	f/2.8	1.25%	1.08%
75mm	f/3.3	1.61%	0.65%
75mm	f/5.6	0.35%	0.48%
75mm	f/11.0	0.24%	0.21%
75mm	f/22.0	0.31%	0.24%
Average		0.84%	0.72%

fitting. Table 1 presents the percentage error of our fitted data from the estimated vignetting effects at these sampled device settings which are also plotted in Figure 2(a). Our average mean error is less than 1% with the average standard deviation being also less then 1%. The low mean and standard deviation from the mean of this error justifies our use of a Bézier representation.

Next, we use the recovered $C(u, v, f', a')$ to predict the vignetting effect at several new device settings. These device settings are shown in Figure 2(b). To parameterize the new device settings parameters to the new normalized parameters, we interpolate the approximation of p_f and p_a using two different techniques.

Global fitting: In the first case, we used the computed (f', a') at *all* device settings where the photometric parameters are measured i.e. $\{(f, a)|f \in \{f_1, f_2, \ldots, f_F\}, a \in \{a_1, a_2, \ldots, a_A\}\}$ (see (Figure 2(a)) to approximate p_f and p_a with a globally fitted 2D Bézier function, as illustrated in. Figure 4. A Bézier of degree 3 was sufficient for this purpose. Next we evaluate this fitted function at the new device parameters (f_{new}, a_{new}) to generate the new normalized parameters (f'_{new}, a'_{new}).

Local fitting: In this we use a local cubic interpolation of the (f', a') to generate the new normalized parameters (f'_{new}, a'_{new}). Thus, in this case the function p_f and p_a are approximated by piecewise cubic patches.

To verify the accuracy of our prediction, we estimate the vignetting at the same device settings and compared it with the predicted vignetting. To recover the photometric properties we use the method presented by [8] for self-calibrating a projector-camera pair. Table 2 and 3 presents the percentage error of our predicted vignetting from the estimated one for the global and local fitting respectively. The results are comparable and both show an average mean error of less than 2% and the average standard deviation from the mean of less the 1.5%. The errors of Table 2 is also plotted with the associated device settings in Figure 2(b). A visual comparison is available in Figure 3 where a captured image is corrected using both the predicted and estimated vignetting. Note that the difference between the two is visually indistinguishable.

Table 2. Percentage error in predicted vignetting using global fitting for interpolating normalized parameters

focal length	f/Stop	Mean	STD
28mm	f/4.0	1.19%	0.90%
28mm	f/8.0	1.75%	1.31%
28mm	f/16.0	2.26%	1.50%
35mm	f/4.0	1.74%	1.51%
35mm	f/8.0	2.46%	1.69%
35mm	f/16.0	3.02%	2.26%
50mm	f/2.8	1.56%	1.03%
50mm	f/3.3	2.04%	2.00%
50mm	f/4.0	2.13%	1.58%
50mm	f/5.6	2.32%	1.38%
50mm	f/8.0	1.26%	0.97%
50mm	f/11.0	1.15%	0.89%
50mm	f/16.0	1.94%	1.27%
50mm	f/22.0	1.61%	1.15%
62mm	f/4.0	1.57%	1.43%
62mm	f/8.0	1.21%	0.81%
62mm	f/16.0	1.17%	0.99%
75mm	f/4.0	1.10%	0.84%
75mm	f/8.0	5.62%	2.89%
75mm	f/16.0	1.60%	0.62%
Average		1.96%	1.35%

Finally, a projector is a dual of a camera [22]. Hence we anticipate our representation, parametrization and prediction to work equally well for a the photometric properties of a projector. However, currently it is difficult to experiment in projectors unless we get digitally controlled zoom and focus capability, only available today in high end projectors. We believe that the same paradigm can be extended to find a compact predictive representation of projector vignetting function as the orientation of the projector with respect to the screen changes or the distance of the projector with respect to the screen changes. Hence, our device independent representation can be applied in other projector and camera related problems. In fact, we use this representation to store

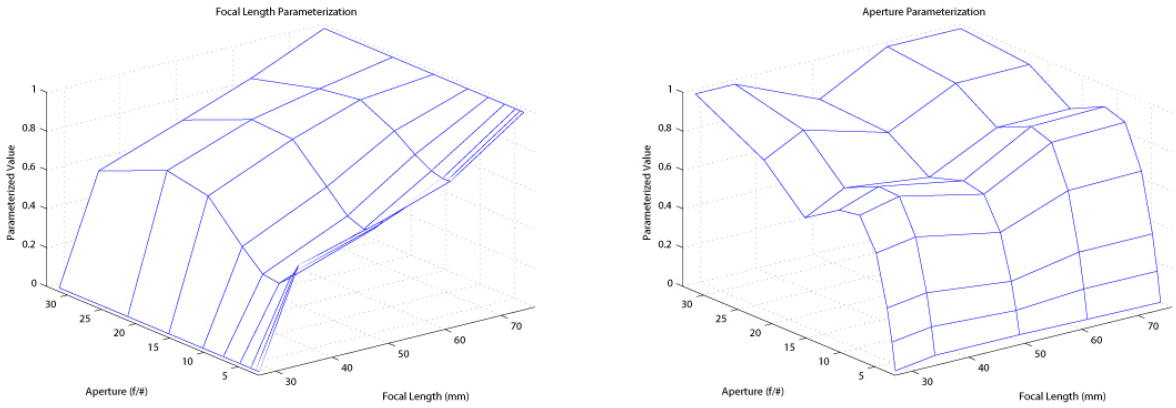

(a) (b)

Figure 4. These shows the plot of the function F_1(a) and F_2(b) respectively corresponding to device parameters aperture and focal length respectively. These are represented using 2D Bézier patches of degree 3.

Table 3. Percentage error in predicted vignetting using local fitting for interpolating normalized parameters.

focal length	f/Stop	Mean	STD
28mm	f/4.0	2.26%	1.13%
28mm	f/8.0	1.71%	1.15%
28mm	f/16.0	4.61%	2.84%
35mm	f/4.0	1.54%	1.10%
35mm	f/8.0	2.39%	1.43%
35mm	f/16.0	4.43%	1.92%
50mm	f/2.8	1.45%	1.06%
50mm	f/3.3	1.28%	1.28%
50mm	f/4.0	2.11%	1.43%
50mm	f/5.6	1.53%	0.86%
50mm	f/8.0	0.94%	0.82%
50mm	f/11.0	0.72%	0.56%
50mm	f/16.0	0.55%	0.65%
50mm	f/22.0	0.57%	0.44%
62mm	f/4.0	1.41%	1.06%
62mm	f/8.0	1.40%	0.93%
62mm	f/16.0	0.51%	0.31%
75mm	f/4.0	1.05%	0.83%
75mm	f/8.0	4.91%	2.73%
75mm	f/16.0	0.27%	0.21%
Average		1.75%	1.10%

our projector vignetting functions for a multi-based display applications [**?**, **?**]. However, we do not use it yet for prediction since we do not have a way to digitally control the settings of our inexpensive commodity projectors.

3.4. Handling Higher Dimensional Device Setting Space

The above representation can be easily generalized for a device settings space that involves more that two parameters. For a M dimensional device settings space spanned by M device parameters $d_1, d_2, \ldots, d_M$, the representation will be a $M + 2$ dimensional Bézier given by $C(u, v, d'_1, d'_2, \ldots, d'_M)$, where $d'_k = p_{d_k}(d_1, d_2, \ldots, d_M), 1 \leq k \leq M$. Also, in this general case, during prediction using global fitting, the d'_k will be approximated using a M dimensional Bézier function

3.5. Discussion

The choice of Bézier surface was motivated by the goal of a general representation. First, Bézier surfaces provides the ability to represent a large number of smooth variations of several orders and dimensions. Thus they are *flexible*. By changing just a single parameter, the degree of the Bézier surface, one can capture the different rate of change in the smoothness of the surface in different devices. Smooth surfaces have a lower degree while surfaces that are not as smooth have a higher degree. Also, as mentioned below the smoothness of the photometric properties can vary differently with different device settings (different parameters of the Bézier) and can also be easily captured by changing the degree of the constituting Bernstein polynomials.

Second, Bézier surfaces provide a very compact representation. For example, in a 6 megapixel camera where the captured images are 3000×2000 pixels, to store the vignetting effect for 100 apertures in a non-parametric representation, one would need to store $100 \times 3000 \times 2000 = 600,000,000$ floating point numbers. If each floating point number occupies 4 bytes, this is 9100 MB. If we resort to a existing parametric notation of polynomial representation

(degree 4), this would need storing $5 \times 100 = 500$ floating point numbers. But, a quadric Bézier surface representation would represent this with only 125 floating point numbers. The compactness is exploited more with the increase in the number of device parameters. This compact representation opens up the possibility of one time calibration (maybe in the factory prior to the sale of the product) and compact storage of photometric properties in the camera itself, maybe in the form of a look-up-table(LUT). Further, one can even imagine storing these properties in the lens itself. Currently, lenses use some small amount of memory to store focal length, aperture and other settings. Our representation, being small, can be accommodated even in such a limited storage.

Finally, the prediction and data-fitting calculations related to a Bézier surface is relatively simple and can be easily embedded in hardware. The Bézier parameters can be embedded as the metadata to the image along with other common parameters like focal length, white balance and so on. The embedded hardware can then automatically correct for the artifacts on-the-fly or can be used for software postprocessing.

4. Conclusion

In conclusion, we have presented a simple device independent representation of the photometric properties of a camera. This opens up the potential of embedding these parameters and a process to correct images using them appropriately within the camera hardware itself.

References

[1] N. Asada, A. Amano, and M. Baba. Photometric calibration of zoom lens systems. *Proceedings of the 13th International Conference on Pattern Recognition*, 1, 1996. 1

[2] C. M. Bastuscheck. Correction of video camera response using digital techniques. *Journal of Optical Engineering*, 26:1257–1262, 1987. 1

[3] Y. P. Chen and B. Mudunuri. An anti-vignetting technique for superwide field of view mosaicked images. *Journal of Imaging Technology*, 12:293–295, 1986. 1

[4] P. E. Debevec and J. Malik. Recovering high dynamic range radiance maps from photographs. *Proceedings of ACM Siggraph*, pages 369–378, 1997. 1, 2, 3

[5] D. Goldman and J. Chen. Vignette and exposure calibration and compensation. *Proceedings of IEEE International Conference on Computer Vision*, pages 899–906, 2005. 1

[6] M. Grossberg and S. Nayar. Determining the camera response from images: What is knowable? *IEEE Transaction on Pattern Analysis and Machine Intelligence*, 25:1455–1467, 2003. 1

[7] M. Grossberg and S. Nayar. Modeling the space of camera response functions. *IEEE Transaction on Pattern Analysis and Machine Intelligence*, 26:1272–1282, 2004. 1

[8] R. Juang and A. Majumder. Photometric self-calibration of a projector-camera system. *IEEE CVPR Workshop on Projector Camera Systems*, 2007. 2, 5

[9] S. Kim and M. Pollefeys. Radiometric self-alignment of image sequences. *Proceedings of IEEE Conference on Computer Vision and Pattern Recognition*, 2004. 1

[10] S. Lin, J. Gu, S. Yamazaki, , and H. Shum. Radiometric calibration from a single image. *Proceedings of IEEE Conference on Computer Vision and Pattern Recognition*, pages 938–945, 2004. 1

[11] S. Lin and L. Zhang. Determining the radiometric response function from a single grayscale image. *Proceedings of IEEE Conference on Computer Vision and Pattern Recognition*, pages 66–73, 2005. 1

[12] A. Litvinov and Y. Schechner. Addressing radiometric nonidealities: A unified framework. *Proceedings of IEEE Conference on Computer Vision and Pattern Recognition*, pages 52–59, 2005. 1

[13] A. Litvinov and Y. Schechner. Radiometric framework for image mosaicking. *Journal of Optical Society of America*, 22:839–848, 2005. 1

[14] A. Majumder and R. Stevens. Color nonuniformity in projection-based displays: Analysis and solutions. *IEEE Transactions on Visualization and Computer Graphics*, 10(2), March–April 2003. 3

[15] S. Mann and R. Mann. Quantigraphic imaging: Estimating the camera response and exposures from differently exposed images. *Proceedings of IEEE Conference on Computer Vision and Pattern Recognition*, pages 842–849, 2001. 1, 2

[16] S. Mann and R. Picard. On being undigital with digital cameras: Extending dynamic range by combining differently exposed pictures. *Proc. IS&T 46th annual conference*, pages 422–428, 1995. 1

[17] V. Masselus, P. Peers, P. Dutre, and Y. D. Willems. Relighting with 4d incident light fields. *Proceedings of ACM SIGGRAPH)*, 2003.

[18] T. Mitsunaga and S. Nayar. Radiometric self calibration. *Proceedings of IEEE Conference on Computer Vision and Pattern Recognition*, 1999. 1

[19] S. K. Nayar, G. Krishnan, M. D. Grossberg, and R. Raskar. Fast separation of direct and global components of a scene using high frequency illumination. *ACM Transactions on Graphics (SIGGRAPH)*, 25(3), 2003.

[20] C. Pal, R. Szeliski, M. Uyttendaele, and N. Jojic. Probability models for high dynamic range imaging. *Proceedings of IEEE Conference on Computer Vision and Pattern Recognition*, pages 173–180, 2004. 1

[21] C. Pinhanez, M. Podlaseck, R. Kjeldsen, A. Levas, G. Pingali, and N. Sukaviriya. Ubiquitous interactive displays in a retail environment. *Proceedings of SIGGRAPH Sketches*, 2003.

[22] R. Raskar, G. Welch, M. Cutts, A. Lake, L. Stesin, and H. Fuchs. The office of the future: A unified approach to image based modeling and spatially immersive display. In *Proceedings of ACM Siggraph*, pages 168–176, 1998. 5

[23] A. A. Sawchuk. Real-time correction of intensity nonlinearities in imaging systems. *IEEE Transactions on Computers*, 26:34–39, 1977. 1

[24] P. Song and T. J. Cham. A theory for photometric self calibration of multiple overlapping projectors and cameras. *IEEE CVPR Workshop on Projector Camera Systems*, 2005. 2

[25] Y. Tsin, V. Ramesh, and T. Kanade. Statistical calibration of the ccd imaging process. *Proc. IEEE International Conference on Computer Vision*, pages 480–487, 2001. 1

[26] M. Uyttendaele, A. Criminisi, S. B. Kang, S. Winder, R. Hartley, and R. Szeliski. Image-based interactive exploration of real-world environments. *IEEE Computer Graphics and Applications*, 24:52–63, 2004. 1

[27] R. Yang, A. Majumder, and M. Brown. Camera based calibration techniques for seamless multi-projector displays. *IEEE Transactions on Visualization and Computer Graphics*, 11(2), March-April 2005.

[28] W. Yu. Practical anti-vignetting methods for digital cameras. *IEEE Transactions on Consumer Electronics*, 50:975–983, 2004. 1

[29] W. Yu, Y. Chung, and J. Soh. Vignetting distortion correction method for high quality digital imaging. *Proceedings IEEE International Conf. on Pattern Recognition*, pages 666–669, 2004. 1

[30] Y. Zheng, S. Lin, and S. B. Kang. Single-image vignetting correction. *Proceedings of IEEE Conference on Computer Vision and Pattern Recognition*, pages 461–468, 2006. 1